Analytical calculation of static leakage inductances of H.F. transformers using PEEC formulas

Xavier Margueron, Jean-Pierre Keradec, David Magot

Analytical Calculation of Static Leakage Inductances of HF Transformers Using PEEC Formulas

Xavier Margueron, Jean-Pierre Keradec, *Member, IEEE*, and David Magot

***Abstract*—When the total current going through a transformer window is equal to zero, only a negligible part of the magnetic energy reaches its core. This is shown by finite-element-method simulations carried out on several two-winding transformers having different shapes. Moreover, induction and energy-density values obtained by 3-D simulations and by 2-D approximations are very close to each other. These two key observations justify the use of formulas that give the induction created by straight rectangular cross-sectional wires, as used in the partial-element-equivalent-circuit method, to compute the window field and, thus, to value the leakage inductances. To refine this approach, weak magnetic-core effects are accounted for by introducing the magnetic images of currents that flow in the windings. A comparison between the calculated values and measured ones is provided.**

***Index Terms*—Analytical calculation, equivalent circuit, leakage inductance, partial-element-equivalent-circuit (PEEC) method, transformer.**

I. Introduction

In SWITCHING power electronics, transformer leakage inductances have a major impact on switching power losses and switches' reliability. Thus, it is important to find their values, before transformer assembling, in order to avoid, or at least to reduce, an expensive prototyping.

Among the parameters needed to run electronic simulations, the leakage inductances of a transformer are not the easiest to forecast. At first sight, there are two ways of computing them: simulation and analytical calculation. Assuming that a device description is detailed enough, simulation leads to accurate results. Unfortunately, device description and modification, as well as simulation itself, are time consuming. Moreover, finite-element-method (FEM) simulation is difficult to manage when running an automatic optimization process, involving the whole circuit [1]. For all these reasons, analytical calculations are welcome.

In the literature, there are mainly two analytical methods proposed for leakage-inductance calculation. The first one is the most commonly used [2], [3]. It neglects one induction component inside the winding window, and it deduces the other one from Ampere's theorem, assuming that current density is uniform in the rectangular cross-sectional windings. This method gives quite good results for windings having very simple geometries. Unfortunately, its extension, even to slightly different layouts, is impossible. In particular, it cannot be applied if some windings or layers have different heights, or when they are not aligned.

The second method uses double Fourier's series expansions [4] to solve Laplace and Poisson's equations inside a rectangular window. This method assumes an induction to be normal to window edges that cannot be fully justified when windings are not completely surrounded by the core. Moreover, because current density is square shaped, the convergence of this expansion is slow. A lot of terms are required to reach a sufficient accuracy.

This paper aims to compute the leakage inductance in a different way. In this goal, magnetic field and energy density in the window are calculated by superposing inductions created by a few straight rectangular wires. Generally, two to five "wires," each accounting for a winding or a part of a winding, lead to accurate values. Obviously, this approach relies on the same basic formulas as partial-element-equivalent-circuit (PEEC) method [5], [6] does. The weak magnetic-core effect is also taken into account, by adding one or eight magnetic images of the windings. One image is used if only one side of the winding window is lined up by the core, and eight images are used, if it is entirely surrounded by the core. Finally, an integration of energy density over space is done analytically. It is investigated for planar and axial geometries. Two industrial transformers are studied in detail in order to check these methods. Obtained results are compared to measurements.

II. Basic Definitions and Formulas

A. Low Frequency Equivalent Circuit of a Transformer

Fig. 1 shows a low-frequency equivalent circuit of a two-winding transformer. This circuit is general, and it avoids splitting the leakage arbitrarily into two parts [7]. If coupling is strong, transformation ratio η is very close to the turn number ratio, and leakage inductance L_f is far smaller than magnetizing one L_m. Studying the input impedance of this circuit when its output is short-circuited shows that L_f is the imaginary part of its HF value. In practice, L_f is read directly on the

Paper IPCSD-06-117, presented at the 2004 Industry Applications Society Annual Meeting, Seattle, WA, October 3–7, and approved for publication in the IEEE TRANSACTIONS ON INDUSTRY APPLICATIONS by the Power Electronics Devices and Components Committee of the IEEE Industry Applications Society. Manuscript submitted for review October 31, 2004 and released for publication February 6, 2007.

The authors are with the Laboratoire d'Electrotechnique de Grenoble, ENSIEG, BP46, UMR 5269, INPG UJF CNRS, 38402 Saint Martin d'Hères Cedex, France (e-mail: Xavier.Margueron@leg.ensieg.inpg.fr; Jean-Pierre.Keradec@leg.ensieg.inpg.fr; magdavb@yahoo.com).

Color versions of one or more of the figures in this paper are available online at http://ieeexplore.ieee.org.

Digital Object Identifier 10.1109/TIA.2007.900449

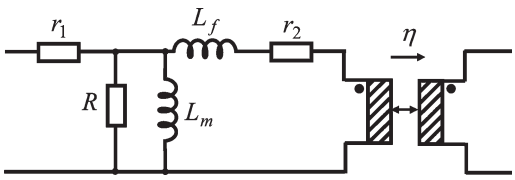

Fig. 1. Low-frequency equivalent circuit of a transformer.

L_s–R_s decomposition of this impedance, at a frequency high enough to avoid the L_m influence and low enough to avoid the stray capacitance effects (not accounted for in this paper) [8]. A measured example is given in Fig. 9. When, exceptionally, coupling is weak, the given circuit is still applicable, but the two-port circuit must be fully characterized to access the L_f value [8].

Now, let us look again to the equivalent circuit (Fig. 1). It appears that supplying the transformer with two currents whose ratio is equal to the transformation ratio cancels the current flowing in L_m if they are correctly orientated. In this case, magnetic energy is entirely stored in L_f. When coupling is strong, the chosen assumptions lead to null the total Ampere turns or, more simply, to null the total current that flows through the window. To sum up, when current I_p is input in the primary and assuming that a total current flowing through the window is null, the energy W stored in the transformer is given by (1). This is the way we will access L_f

$$W = \frac{1}{2} L_f \cdot I_p^2. \tag{1}$$

As mentioned in the title, in this paper, we only look for the static values of leakage inductances, that is to say, values that are obtained at frequencies that are low enough for the eddy currents to be negligible. In practice, as frequency grows, the leakage inductances slightly decrease and the series resistances increase. We have already investigated these phenomenon experimentally, and we introduced parallel cells L_p–R_p to account for them in the equivalent circuit [8]. Indeed, relative variations of leakage inductances are quite small. Therefore, the calculation presented here supplies the designer with a first approximation which is accurate as long as the eddy-current effects remain weak.

B. Leakage Energy Calculation

As justified previously, L_f is computed by identifying the energy stored in the transformer to that stored by the L_f, when the total Ampere turns is null. The whole calculation process can be split into several stages, which are presented next.

To begin, induction and vector potential are computed inside the transformer window. This will be detailed further on. Because we only consider devices such that any plan normal to the wires is a symmetry plan, the induction is parallel to this plan and the vector potential is normal to this plan. None of these fields varies along wire direction.

At this stage, the energy per unit of length parallel to the wires wl is deduced from expressions (2) or (3). It is a relevant

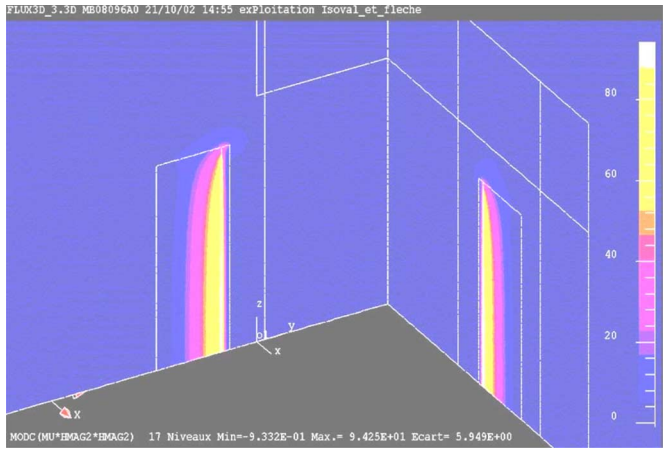

Fig. 2. Energy density in an EP 13 ferrite core transformer.

parameter to check field accuracy

$$wl = \frac{1}{2\mu_0} \int \int B^2(x,y) dx dy \tag{2}$$

$$wl = \frac{1}{2} \int \int \vec{A}\,\vec{J}\, dx dy. \tag{3}$$

Theoretically, the first integral (2) must extend to infinity. In practice, we bound it to the window area to save computer memory. The second integral (3) is bounded to the current area, and that is more convenient. Supposing that the current density is constant in every rectangular winding or wire cross section, this parameter can be placed in factor of the integral. Thus, the integral can be analytically calculated.

The energy stored in the whole component is found by integrating its energy density wl. If wires are straight, then the energy per unit of length given by formulas (2) and (3) is simply multiplied by the mean turn length. However, if left and right windows are different, one half of the mean turn length is supposed to store each of the calculated energy densities. For cylindrical windings, energy densities are first integrated parallel to symmetry axis (Oy). Then, a second integration accounts for real wire length, which is proportional to polar radius r. This way, (2) leads to (4). For complex geometries, straight sections can be mixed with cylindrical ones

$$W = \frac{1}{2\mu_0} \int \left[\int B^2(r,y) dy \right] 2\pi r dr. \tag{4}$$

C. Observations and Induced Approximations

An EP core is mainly a cylindrical pot having internal and external legs. However, this core is cut tangentially to the internal leg. Consequently, windings are only partly surrounded by the core. An EP 13 ferrite core transformer, with an external winding that is eight times thicker than the internal one, has been studied with FEM software [9]. Fig. 2 shows the energy density obtained when the total current in the window is null. Only the upper half of this transformer is presented. Two perpendicular cross sections are shown. On the left-hand side, windings are outside the core, whereas they are inside on the right-hand side.

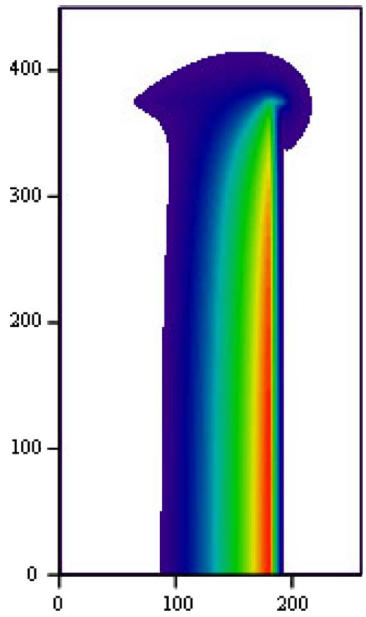

Fig. 3. Analytical calculation of energy density of a pair of straight rectangular cross-sectional wires carrying uniform current densities.

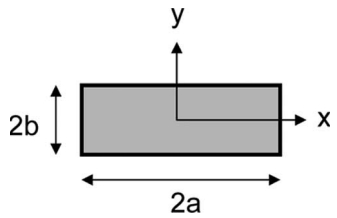

Fig. 4. Rectangular wire.

Two interesting properties appear. First, energy density is negligible in the core. Referring to color scale, it is, at least, 20 times lower in the core than at its maximum. Second, densities on the two orthogonal cross sections are almost equal, despite that one is surrounded by the core and the other is not. This observation suggests that core is not of significant importance in the leakage-inductance computation.

Moreover, when the thickness of a winding is smaller than its mean radius, the induction it creates is logically close to that which would exist if it was unwound. This simpler description allows analytical calculation to be carried out. The energy density due to the two rectangular wires carrying a null total current (Fig. 3) looks like that shown in Fig. 2. This reinforces the two previous hypotheses.

In the following, we will assume that the winding window includes a few rectangular areas carrying homogenous current densities.

D. PEEC Formulas

Our elementary field source is an infinite straight wire, having a rectangular cross section (Fig. 4), in which a homogenous current flows.

Vector potential (5) can be obtained by integrating that of a thin wire, from $x=-a$ to $+a$ and from $y=-b$ to $+b$. However, this potential is among the more widely involved by the PEEC method [5], [6], except that source wire is assumed here to be infinitely long. Rectangular components of induction (6) and (7) are deduced from the vector potential (5) through proper derivatives.

$$\begin{aligned} A_z(x,y) &= \frac{-\mu_0 \cdot I}{4\cdot\pi\cdot(2\cdot a\cdot 2\cdot b)} \\ &\quad\cdot\left[\left[\left[XY\ln(X^2+Y^2)+X^2\arctan\left(\frac{Y}{X}\right)\right.\right.\right. \\ &\qquad\left.\left.\left.+Y^2\arctan\left(\frac{X}{Y}\right)\right]_{X=x+a}^{X=x-a}\right]_{Y=y+b}^{Y=y-b}\right] \end{aligned} \tag{5}$$

$$\begin{aligned} B_x(x,y) &= \frac{\mu_0 I}{16\cdot\pi\cdot a\cdot b} \\ &\quad\times\left[2(y-b)\left(\arctan\left(\frac{x+a}{y-b}\right)-\arctan\left(\frac{x-a}{y-b}\right)\right)\right] \\ &\quad-2(y+b)\left(\arctan\left(\frac{x+a}{y+b}\right)-\arctan\left(\frac{x-a}{y+b}\right)\right) \\ &\quad+(x+a)\ln\left[\frac{(x+a)^2+(y-b)^2}{(x+a)^2+(y+b)^2}\right] \\ &\quad+(x-a)\ln\left[\frac{(x-a)^2+(y+b)^2}{(x-a)^2+(y-b)^2}\right] \end{aligned} \tag{6}$$

$$\begin{aligned} B_y(x,y) &= \frac{-\mu_0 I}{16\cdot\pi\cdot a\cdot b} \\ &\quad\times\left[2(x-a)\left(\arctan\left(\frac{y+b}{x-a}\right)-\arctan\left(\frac{y-b}{x-a}\right)\right)\right] \\ &\quad-2(x-a)\left(\arctan\left(\frac{y+b}{x+a}\right)-\arctan\left(\frac{y-b}{x+a}\right)\right) \\ &\quad+(y+b)\ln\left[\frac{(x-a)^2+(y+b)^2}{(x+a)^2+(y+b)^2}\right] \\ &\quad+(y-b)\ln\left[\frac{(x+a)^2+(y-b)^2}{(x-a)^2+(y-b)^2}\right]. \end{aligned} \tag{7}$$

When Nc wires are considered together, resulting induction is computed as the sum of all individual fields properly shifted by (x_k, y_k), according to (8) and (9)

$$B_x(x,y)=\sum_{k=1}^{Nc}\left[B_{x_k}(x-x_k,y-y_k)\right] \tag{8}$$

$$B_y(x,y)=\sum_{k=1}^{Nc}\left[B_{y_k}(x-x_k,y-y_k)\right]. \tag{9}$$

From (8) and (9), it can be shown that, for flat windings stuck by their small side, energy is not located close to the common side, so that the one component (common) approximation of the induction [2], [3] is no longer justified.

E. Magnetic Images

Let us consider a thin straight wire (Fig. 5) that carries a current I, parallel to the plane interface bounding two materials of respective relative permeability 1 and μ_r.

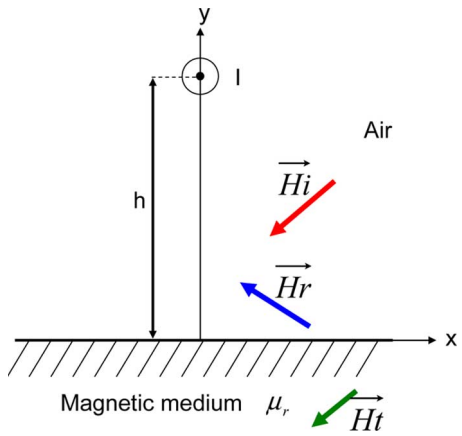

Fig. 5. Induction created by a thin wire located above a magnetic material.

In the magnetic material, excitation Ht is simply multiplied by coefficient (10). In the air, it is now the sum of the one (Hi) created by the wire alone and another (Hr) created by another wire, which is called "image wire" [10], symmetrically located on the other side of this interface, and through which a current given by (11) flows

$$\frac{2}{\mu_r + 1} \tag{10}$$

$$I\frac{\mu_r - 1}{\mu_r + 1}. \tag{11}$$

If μ_r is far greater than 1, the current carried by the image wire is equal to that of the initial wire. In this case, at the interface, tangential component of the induction vanishes, whereas perpendicular one doubles. When μ_r is not very high, the density of image current is a little bit smaller: it must be tuned according to (11). Extension to a set of parallel wires and to a parallel continuous current distribution is obvious, and induction in air is the sum of those created by both the initial current distribution and its images.

It must be underlined that, despite the vector-potential field created by a symmetrical current distribution is symmetrical to the initial one, this is not true for the induction field. It is due to the pseudovector nature of the flux density. Adding initial and image inductions requires, therefore, to add the normal components and to subtract the tangential ones.

F. Numerical Integration

In order to check the realism of our calculated fields, we will compare them to those obtained by the FEM simulations. This introduced some special constraints. Because FEM simulation only gives numerical values of fields, energy evaluation must be carried out by the way of a numerical integration. In order to compare the FEM simulation to the analytical calculation and to get an information about the numerical precision achieved, we used the same algorithm in both cases. A fixed grid is therefore applied to the rectangular area of interest. Then, the energy per length unit is computed as the sum of the energies stored in every grid element. In each elementary rectangular element of surface $dS = dx \cdot dy$, the energy density is chosen equal to the mean of the four values that are taken at the corners of this element. Then, N_x and N_y being the numbers of elements in the x-and y-directions, the energy per unit of length is expressed as (12) rather than (2)

$$wl = \frac{dS}{2\mu_0}\sum_{i=1}^{N_x}\left[\sum_{j=1}^{N_y}\frac{B_{i,j}^2 + B_{i-1,j}^2 + B_{i,j-1}^2 + B_{i-1,j-1}^2}{4}\right]. \tag{12}$$

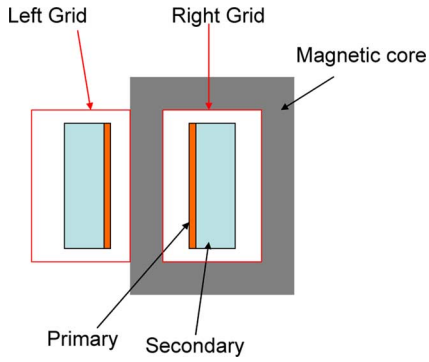

Fig. 6. 2-D representation of an EP core transformer.

III. EP Ferrite Core Transformer

Now, let us return to our EP core transformer. As stated before, Fig. 2 suggests several approximations. We are now going to check each of them carefully.

A. Device Description

This device (Fig. 6) is an insulation transformer, which is built from an EP13 core made of 3C90 ferrite. Both windings have 46 turns. The primary is wound on a little bit more than one layer, with an enameled copper. The wire diameter is 0.15 mm, with a copper diameter of 0.125 mm. The secondary is made of about three layers of polyamide insulated copper. Wire and copper diameters are 0.4 and 0.2 mm, respectively. As already mentioned, windings are outside the core on the left-hand side of Fig. 2, despite that they are inside it on the right-hand side.

For this component, windings are simply described as adjacent rectangular homogenous current densities, with zero total current for the leakage-inductance evaluation. This simplified description has been used for the 2-D simulations presented next.

B. Calculation of Energy Per Length Unit

Two formulas (2) and (3) are available to calculate this value. The integration of (2) will be extended to the window area, and the left window area boundaries will be assumed to be symmetrical to that of the right window. Calculation is carried out according to (12). Unlike the use of (3), using (2) does not require any grid update when the conductor sizes or numbers are changed.

However, in order to check the reliability of values found this way, we applied both formulations to the 2-D simulated fields. Table I shows that the two computations lead to almost the same results. The value coming from $\overrightarrow{A}\,\overrightarrow{J}$ integration (3),

TABLE I
COMPARING THE TWO METHODS OF ENERGY CALCULATION

	Left window	Right window
BH Integ	71.24 μJ/m	73.82 μJ/m
AJ Integ	71.90 μJ/m	73.92 μJ/m

TABLE II
ENERGY PER LENGTH UNIT EVALUATED IN 2-D AND 3-D

	Left window	Right window
3D	67.4 μJ/m	70.0 μJ/m
2D	71.2 μJ/m	73.8 μJ/m

which is the energy in the whole space, is a little bit larger than that based on $\vec{B}\,\vec{H}$ integration (2), and due to the lack of surrounding ferrite, energy is a little bit more spread in the left window.

C. Impact of Core and Winding Curvature

This transformer has been simulated in 3-D, and its windings have been described as the adjacent rectangular homogenous current densities with opposite but equal currents in both windings. As in Fig. 2, the left window is outside the core. In order to evaluate a curvature impact, we also carried out 2-D simulations (Fig. 6) with the same software.

Table II shows the energies per length unit, which are computed according to (12). The presented results justify our main assumptions. Indeed, by comparing the two columns, it appears that the magnetic-core impact is within 3.5% in 3-D as in 2-D. Comparing now the two lines also shows that the relative curvature effect is about (5%).

D. Comparison With PEEC and Standard Evaluations

Because core and curvature play minor roles, PEEC formulas seem to be usable. Indeed, Fig. 3 looks like Fig. 2, and according to (6) and (7), the energy per length unit is equal to 63.0 μJ/m that is not so far from the values in Table I. For this standard geometry, the common "one component approximation" [2], [3] leads also to a rather good result: 79.8 μJ/m. Fig. 7 shows the vertical (main) induction component on two paths: at the interface (a) between the two windings and (b) along the horizontal symmetry plane. In Fig. 8(a), windings end at 3.75 mm, and in Fig. 8(b), winding limits are at -0.75 and 0.6 mm.

Despite a rather good curve shape agreement, the analytical model fails in calculating the values that are close to the window edges, and this leads to a downshift of the whole curve. This slight discrepancy is due to the magnetic core that pulls the tangential component toward zero against the window edges.

E. Accounting for Magnetic Core

In our tables, accounting for the magnetic core is referred to as PEEC+, and this is done differently for both windows

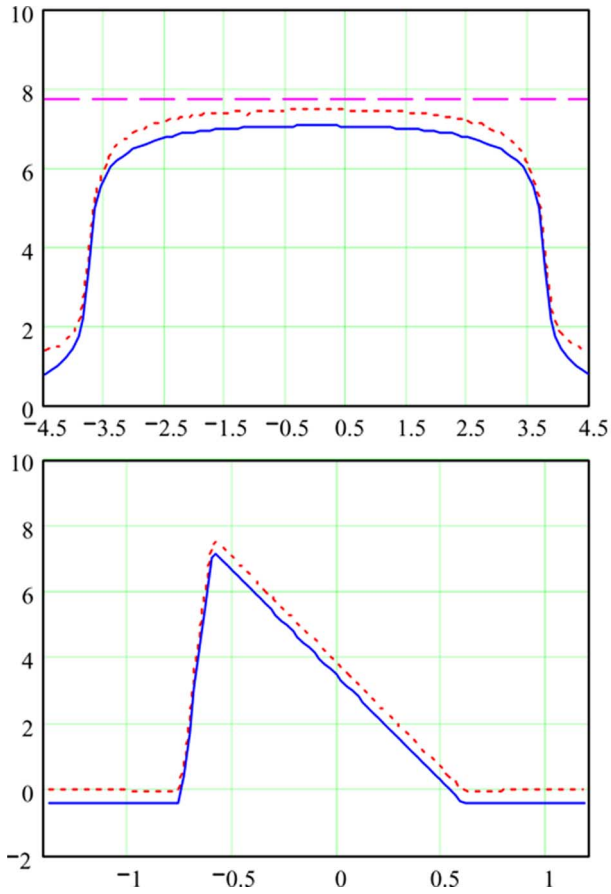

Fig. 7. Induction (in mT) versus coordinates (in mm) in the right window. Dotted line: 2-D simulation. Solid line: Analytical. Dashed line: "One component" approximation. (a) At the interface between the windings. (b) Along a horizontal line in the middle of the window.

(Fig. 6). For the left-hand side, only one magnetic image is introduced on the right-hand side of the window

$$Bc_x(x,y) = B_x(x,y) + B_x(2\cdot x\mathrm{rw} - x, y)$$
$$Bc_y(x,y) = B_y(x,y) - B_y(2\cdot x\mathrm{rw} - x, y). \qquad (13)$$

Above, B and Bc refer to the initial induction and to the global induction, respectively. We also introduced $x$rw as the x coordinate of the right edge of the window.

Because the right window is surrounded by the core, multiple reflections occur, which result in an infinity of images. Fortunately, each one is flown by currents, whose sum is equal to zero. The first term of the multipolar expansion is thus dipolar and, as a consequence, induction decreases fast with distance. For this reason, we only keep the eight closest images. This is carried out through two steps, with formulas similar to (13). We first add two vertical images to the initial current distribution. Then, we add two horizontal images of the previously obtained system.

Fig. 8 shows the improvement brought by this add-on, particularly evident close to the edges of the window. Everywhere on the window edges, the agreement is as good as it appears in Fig. 8(b). The energy per length unit (Table III) shows that the value for left window is now quite perfect, but that a slight overevaluation appears for the right window.

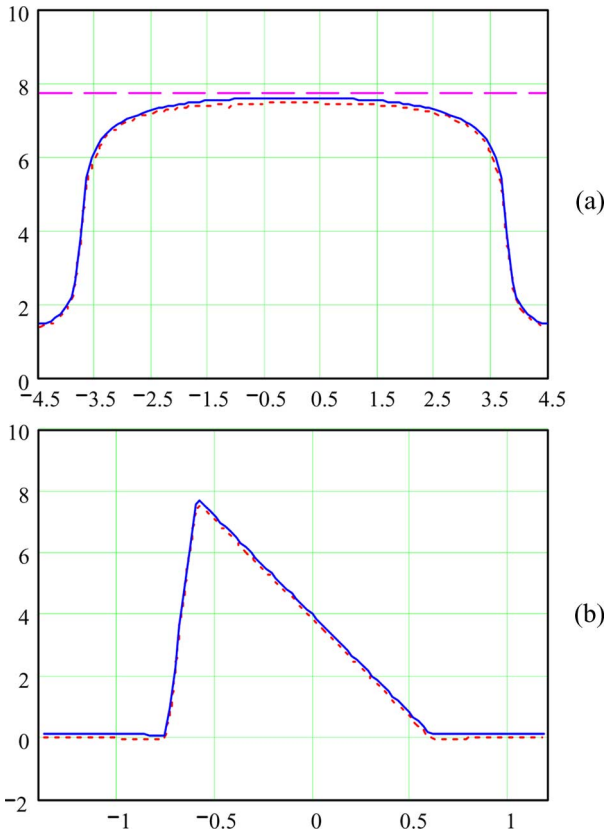

Fig. 8. Same as Fig. 7, but accounting for the magnetic core.

TABLE III
ENERGY PER LENGTH UNIT. COMPARISON BETWEEN THE FEM SIMULATION AND THE ANALYTICAL CALCULATIONS

	Left window	Right window
2D fem	71.2 µJ/m	73.8 µJ/m
PEEC alone	63.0 µJ/m	
PEEC +	70.8 µJ/m	77.2 µJ/m

F. Leakage-Inductance Evaluation and Measurement

Owing to the previous field calculation, the energy stored in the whole device can be computed, and the leakage inductance can be evaluated. In order to have a reference value, we first measured (Fig. 9) its value as explained in Section II-A. We found 3.4 μH. This measurement was carried out with an HP4194A impedance analyzer [11].

Because EP cores have a cylindrical central leg, the energy W stored by the device is computed using cylindrical coordinates. Let r_0 be the radius to the origin of the rectangular coordinates used before. According to (4), the energy is given by (14)

$$Bm_{i,j}^2 = \frac{B_{i,j}^2 + B_{i-1,j}^2 + B_{i,j-1}^2 + B_{i-1,j-1}^2}{4}$$

$$W = \frac{1}{2\mu_0} \sum_{i=1}^{N_x} \sum_{j=1}^{N_y} Bm_{i,j}^2 2\pi \left(r_0 + \frac{x_i + x_{i-1}}{2} \right) dS. \tag{14}$$

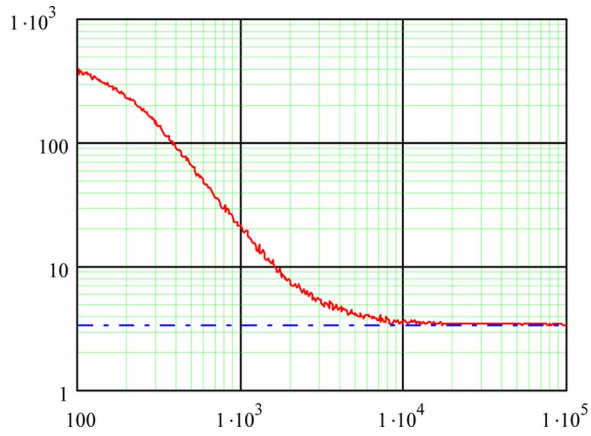

Fig. 9. Series inductance in microhenrys versus frequency in hertz.

TABLE IV
CALCULATED INDUCTANCES. COMPARISON OF SEVERAL EVALUATIONS FOR THE STUCK AND SEPARATED WINDINGS

	Initial geometry	With air gap
2D fem	3.07 µH	NA
PEEC	2.61 µH	2.93 µH
PEEC +	3.21 µH	3.58 µH
Common approx.	3.97 µH	4.51 µH

EP cores are closed on a large part of their circumference. For this reason, we used the induction in the right window, which should lead to a value slightly too high. The results are given in column 2 of Table IV. Despite that fields are accurate compared to simulations, the inductance values are too low, compared to the measurements (3.4 μH). A conclusion arises: The model of the device is too rough. In particular, it neglects the insulator thickness of both wires which introduces an air gap between the two windings.

To check the impact of this air gap, we removed, accordingly to the insulator thickness, 0.1 mm all around the thicker winding and 12.5 μm around the other one, without any other changes. Results are given in column 3 of Table IV. This small change induces a 10% change on the final value. Obviously, this air-gap thickness has a great impact on final precision and PEEC+ calculation is now close to measurement. The common one component approximation, which overestimates induction except on symmetry plan [Fig. 8(a)], gives a value too high in both cases.

The study of this device shows, therefore, that the proposed approach gives accurate results, provided that the winding shapes are precisely described, particularly where the energy density is the highest.

IV. PLANAR TRANSFORMER

A. Device Description and Measured Leakage Inductance

The other studied device is a 250-VA planar transformer working at 200 kHz. It owns three windings and is about 7-mm thick. Its left window is shown in Fig. 11. All wires are

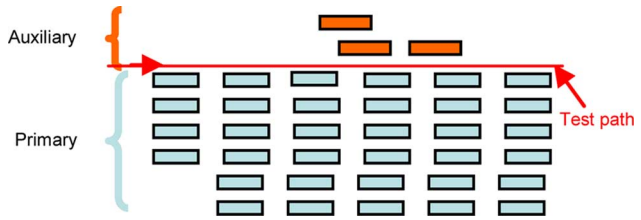

Fig. 10. Left window of the planar transformer.

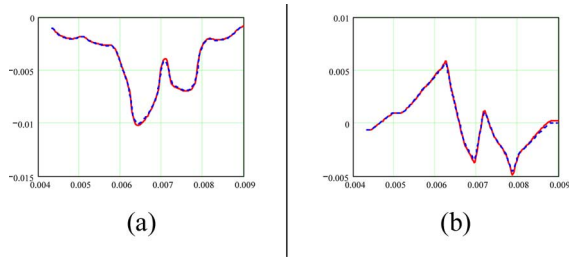

Fig. 11. Induction along the test path. Solid line: 2-D simulated. Dotted line: Calculated. (a) Tangential component. (b) Normal component.

made of copper, have rectangular cross sections, and are parts of a printed circuit board. Primary is made of 17 turns; each is composed of two wires connected in parallel. Secondary, which is not considered in this paper, is not represented for industrial reasons. Third winding, which is the auxiliary, has three turns. We now focus on the leakage inductance between the primary and auxiliary windings. For such a layout, one component approximation is unusable to compute the field. Searched leakage inductance has been measured as 112 nH ($\pm$8 nH due to the measurement precision).

B. PEEC Field Computation

While the secondary remains open, the primary is supplied with a current $I_p = 1$ A, and the auxiliary is supplied with a current $I_a = -17/3$ A, in order to null the total current in the window. In this first approach, magnetic field is evaluated considering each wire as an elementary source of field.

We will now focus on the energy per length unit. A 2-D FEM simulation gives 28.1 μJ/m, whereas the PEEC calculation leads to 28.2 μJ/m, before introducing any image. The sum was computed only in the transformer window. If it is extended to a larger area, a limit equal to 30 μJ/m appears which coincides with the value deduced from the vector potential. Therefore, one can conclude that 93% of the energy is concentrated in the transformer window.

This quite perfect result is reinforced by the observation of the induction shape along a significant test path, located between the primary and auxiliary windings (Fig. 10). The tangential B_x and normal B_y components along this path are given in Fig. 11.

C. Leakage-Inductance Computation Method

As soon as the energy per length unit is known, it remains to multiply it by the mean turn length to obtain the total energy, leading to the inductance value. It must be specified

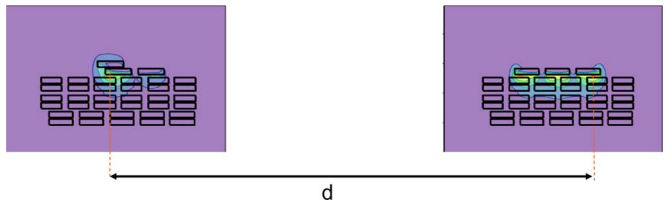

Fig. 12. Distance between the peaks of energy density.

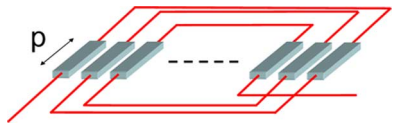

Fig. 13. Mean-turn-length evaluation. P is the core depth.

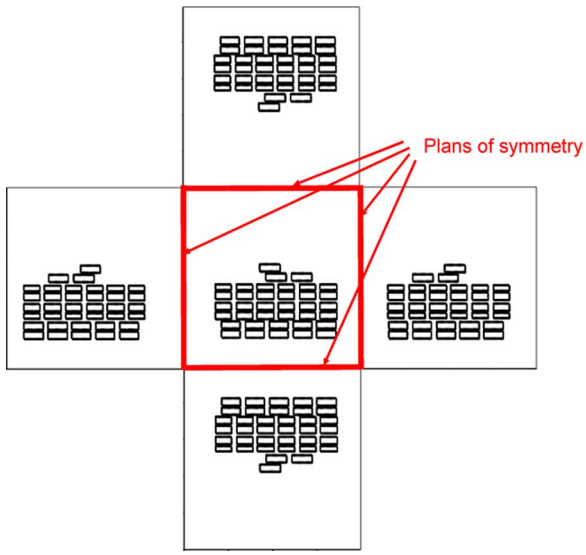

Fig. 14. Magnetic images of the left window.

that, in this component, the magnetic core fully covers all the turns. Because energy density exhibits a sharp peak, using the length corresponding to this peak location, instead of the mean turn length, seems to be more adequate. This has been done here. Referring to Figs. 12 and 13, the mean turn length P is evaluated as $P = 2(d + p)$.

Moreover, because wire layouts are different in the left and right windows (Fig. 12), they are studied separately before the total energy computation. Knowing the energy per length unit in both windows (wll and wlr), we use their average values to compute the total energy stored in the component and, then, the leakage inductance value. Because the energy sum is bounded to the transformer window, this result will likely be slightly minored. Despite that the measured value is 112 nH ($\pm$8 nH), the aforementioned calculation gives 115 nH.

D. Influence of the Magnetic Core

A 2-D simulation has been carried out. Despite that the field initially calculated seemed correct, it was not really accurate at window boundaries when magnetic material is present. To improve model accuracy, we introduced only four images of initial wires (Fig. 14). Owing to this, the field became very close

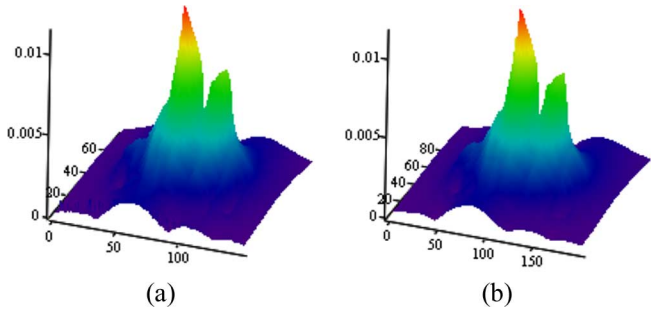

Fig. 15. Field modulus with magnetic core. (a) 2-D FEM simulation. (b) Analytical calculation with images.

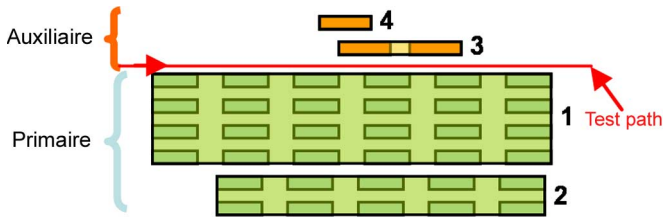

Fig. 16. Homogeneization of rectangular wires.

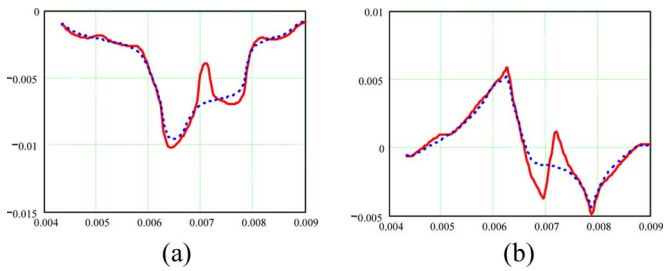

Fig. 17. Induction along the test path. Solid line: full analytical. Dotted line: analytically homogenized. (a) Tangential component. (b) Normal component.

to the simulated one (Fig. 15). For clarity reasons, horizontal and vertical scales have not been respected in this figure.

E. Geometry Simplification Using Homogeneization

The results presented previously about this transformer rely on a detailed geometrical description of the device. In order to shorten both boring data handling and computation time, we try a geometrical simplification. Wires are gathered in four rectangular zones (Fig. 16), and the total current crossing each of them is spread out to obtain homogenous densities.

This smoothens the induction calculated along the test path (Fig. 11) a little bit (Fig. 17). However, the energy per length unit keeps almost the same value: 27.5 μJ/m inside the window compared to 28.2 μJ/m, and 29 μJ/m for the extended area instead of 30 μJ/m.

F. Vector Potential

Theoretically, the energy density must be integrated over the whole space to calculate the leakage inductance. Even if we found that the main part of this energy is stored in the window area, particularly when the winding is fully surrounded by the core, the way to easily reach this limit value is to use the potential vector (5) according to (3). This way of proceeding has been applied to the left window of our transformer. On the rectangular cross sections of all wires, the vector potential is integrated and, then, multiplied by the corresponding current. When applied to the simplified geometry, this leads to 29.7 μJ/m which is very close to the value (30.0 μJ/m) obtained by integrating the induction-based formula over an extended area. Other tries show similar agreement.

Last but not least, in such a case, the involved basic formulas (3) are analytically integrated [12].

G. About Calculation-Measurement Agreement

Measuring the leakage inductance of a transformer, which is always far smaller than the magnetizing one, is sometimes difficult. In particular, when the studied inductance is seen from a low voltage winding, it can be 20 nH or less. With such low values, two questions arise: What is calculated and what is measured? During the calculation, the wires linking turns (inside the core) to component terminals are not taken into account. During the measurement, the wires that are used to connect the component to the impedance analyzer intervene more or less on the result, even if careful short-circuit compensation is used.

Measuring this inductance from the other winding requires null impedance short circuit which is, of course, unavailable. All these parasitic inductances and their possible couplings lead to severe discrepancies between calculation and measurement. As an example, the leakage inductance between the primary and secondary windings of our planar transformer has been evaluated to 6 nH from the calculation and to 20 nH from the measurement. There is still a long way to go before discrepancies disappear durably at this level of inductance.

V. Refining the Image Technique

In most of the practical cases, the impact of magnetic core on searched value is weak so the use of image technique, as presented in Section II-E, allows its evaluation with a sufficient accuracy. However, this technique relies on an assumption: Magnetic medium is supposed infinitely thick.

We investigated the influence of magnetic core thickness ep on the result. To sum up, we can say that magnetic core behaves as an infinite medium when its thickness is beyond a value which decreases when its permeability increases.

To get an order of magnitude, as in [13], we studied a simple system that is composed of a plane finite-thickness magnetic layer and a thin straight wire parallel to its surface. In the air surrounding the wire, magnetic field varies from the minimum obtained without the magnetic layer to the maximum which is reached, for a given permeability, for an infinite thickness. The difference between these two values characterizes the impact of the magnetic layer. When thickness is finite, for $\mu = 2000$, 90% of this impact is obtained for ep $= 1$ mm. With $\mu r = 40$, this figure reaches 20 mm. Therefore, for a high permeability material, our simple image approach is reliable, even for millimetric thickness. For a low permeability material, a series of 20 to 30 images is needed to reach the same accuracy.

When magnetic core does not behave as an infinite media, the current flowing in the opposite window can modify the calculated field. In such a situation, one must consider simultaneously not only a higher number of images to account for multiple reflections in core thickness but also all the field sources located in the two windows.

VI. Conclusion

Based on the formulas used for the PEEC method, a new analytical computation of leakage inductance has been presented. This calculation method suits to evaluate not only all the leakage inductances but also any coupling of them. Therefore, the whole leakage transformer defined in [7] can be studied this way.

Used alone, PEEC formulas lead to a rather good approximation of both field shapes and leakage inductances. If necessary, the magnetic core is taken into account, using the magnetic image technique. By doing so, the impact of the magnetic core can be evaluated, whatever its permeability is, and even if some sides of the winding window are not bounded by the magnetic material (or if they have different permeabilities). As with the FEM simulations, the accuracy of final result heavily relies on the knowledge of some geometrical parameters such as interwinding air-gap thickness, which are sometimes difficult to evaluate.

Two transformers have been investigated. Computed fields are in good agreement with those obtained by the 2-D or 3-D simulations, and values obtained for leakage inductances are within a few percent of measured ones. However, for the leakage inductances below a few tens of nanohenry, an agreement with measured values becomes random. Indeed, the measured values are global, and sharing them between device and wiring is uncertain. Such a situation often occurs for low-voltage power transformers.

The investigated method of computation can be used as a part of an optimization process. Because the vector potential is analytically integrated, this method really leads to analytical expressions that are quickly computed. Moreover, the data set involved can be reduced by using the simple homogenization technique presented.

References

[1] E. Atienza, J. Bigeon, F. Wurtz, and V. Leconte, "EDEN: A generic integrated component software for constraint optimization," in *Proc. 13th Conf. Compumag*, Evian, France, Jul. 2–5, 2001, pp. 232–233.

[2] A. Dauhajre and R. D. Middlebrook, "Modelling and estimation of leakage phenomena in magnetic circuits," in *Proc. 17th Annu. IEEE PESC*, 1986, pp. 213–226.

[3] J. P. Ferrieux and F. Forest, *Alimentations à Découpage, Convertisseurs à Résonance*, 2nd ed. Paris, France: Masson, 1985.

[4] K. J. Binns, P. J. Lawrenson, and C. W. Trowbridge, *The Analytical and Numérical Solution of Electric and Magnetic Fields*. Hoboken, NJ: Wiley, 1992.

[5] A. E. Ruehli, "Survey of computer aided electrical analysis of integrated circuit interconnections," *IBM J. Res. Develop.*, vol. 23, no. 6, pp. 626–639, Nov. 1979.

[6] E. Clavel, J. Roudet, and A. Foggia, "Electrical modeling of transformer connecting bars," *IEEE Trans. Magn.*, vol. 38, no. 2, pp. 1378–1382, Mar. 2002.

[7] X. Margueron and J.-P. Keradec, "Design of equivalent circuits and characterization strategy for n-input coupled inductors," in *Conf. Rec. IEEE IAS Annu. Meeting*, Seattle, WA, Oct. 2004, CD ROM.

[8] X. Margueron and J.-P. Keradec, "Identifying the magnetic part of the equivalent circuit of a n-winding transformer," *IEEE Trans. Instrum. Meas.*, vol. 56, no. 1, pp. 146–152, Feb. 2007.

[9] Cedrat, *Flux*, Meylan, France. [Online]. Available: http://www.cedrat.com

[10] W. A. Roshen, "Analysis of planar sandwich inductors by current images," *IEEE Trans. Magn.*, vol. 26, no. 5, pp. 2880–2887, Sep. 1990.

[11] *Agilent 4294A Precision Impedance Analyser—Operation Manual*, Agilent Technologies, Palo Alto, CA, 2003.

[12] X. Margueron, J.-P. Keradec, and A. Besri, "Complete analytical calculation of static leakage parameters. Application to planar HF transformer optimization," in *Conf. Rec. IEEE IAS Annu. Meeting*, New Orleans, LA, Sep. 23–27, 2007. to be published.

[13] W. A. Roshen, "Effect of finite thickness of magnetic substrate on planar inductors," *IEEE Trans. Magn.*, vol. 26, no. 1, pp. 270–275, Jan. 1990.

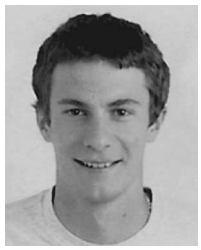

Xavier Margueron was born in Chambery, France, in 1980. He received the diploma of electrical engineering from the Ecole Nationale Supérieure d'Ingénieurs Electriciens de Grenoble, Saint Martin d'Hères, France, in 2003 and the Doctorat de Génie Electrique from the Université de Grenoble, Grenoble, France, in 2006.

He is currently with the Laboratoire d'Electrotechnique de Grenoble, Saint Martin d'Hères, France. He is interested in HF transformer modeling, HF power electronics, and power network safety.

Jean-Pierre Keradec (M'92) was born in Paris, France, in 1947. He received the Doctorat de Physique du Solide from the Université de Grenoble, Grenoble, France, in 1973.

He currently teaches analog electronics, signal processing, and measurement system design at the Institut Universitaire de Technologie de Grenoble and at the Institut National Polytechnique de Grenoble. He has been with the Laboratoire d'Electrotechnique de Grenoble, Saint Martin d'Héres, France, since 1985, and his research interests mainly include HF magnetic components and measurement related to HF power electronics.

David Magot was born in Beaune, France, in 1977. He received the diploma of electrical engineering from both the Ecole Nationale Supérieure d'Ingénieurs Electriciens de Grenoble, Saint Martin d'Hères, France, and the University of Glasgow, Glasgow, U.K., in 2003, and the Doctorat de Génie Electrique from the Institut National Polytechnique de Grenoble, Grenoble, France, in 2006.

He is currently with the Laboratoire d'Electrotechnique de Grenoble, Saint Martin d'Héres, France. He is principally interested in simulation and computer-aided design software.